Title

Uner Tan syndrome caused by a homozygous TUBB2B mutation affecting microtubule stability.

Journal

Human Molecular Genetics, 26(2)

ISSN

0964-6906

Authors

Breuss, Martin W
Nguyen, Thai
Srivatsan, Anjana
et al.

Publication Date

2017-01-15

DOI

10.1093/hmg/ddw383

Peer reviewed

OXFORD

Human Molecular Genetics, 2017, Vol. 26, No. 2 258–269

doi: 10.1093/hmg/ddw383
Advance Access Publication Date: 23 December 2016
Original Article

ORIGINAL ARTICLE

Uner Tan syndrome caused by a homozygous *TUBB2B* mutation affecting microtubule stability

Martin W. Breuss[1,2], Thai Nguyen[1,2], Anjana Srivatsan[3], Ines Leca[4], Guoling Tian[5], Tanja Fritz[4], Andi H. Hansen[4,†], Damir Musaev[1,2], Jennifer McEvoy-Venneri[1,2], Kiely N. James[1,2], Rasim O. Rosti[1,2], Eric Scott[1,2], Uner Tan[6], Richard D. Kolodner[3,7], Nicholas J. Cowan[5], David A. Keays[4] and Joseph G. Gleeson[1,2,*]

[1]Department of Neurosciences, Howard Hughes Medical Institute, University of California, San Diego, La Jolla, CA, USA, [2]Rady Children's Institute for Genomic Medicine, San Diego, CA, USA, [3]Ludwig Institute for Cancer Research, University of California School of Medicine, San Diego, La Jolla, CA, USA, [4]Research Institute of Molecular Pathology (IMP), Vienna Biocenter (VBC), Vienna, Austria, [5]Department of Biochemistry and Molecular Pharmacology, New York University Langone Medical Center, New York, NY, USA, [6]Department of Physiology, Medical School, Cukurova University, Adana, Turkey and [7]Department of Cellular and Molecular Medicine, Institute for Genomic Medicine and Moores-UCSD Cancer Center, San Diego, La Jolla, CA, USA

*To whom correspondence should be addressed at: Joseph G. Gleeson, 9500 Gilman Dr., CNCB 122, La Jolla, 92093-0752, California, USA. Tel: 858-246-0524; Fax: 858-534-8980; Email: jogleeson@ucsd.edu

Abstract

The integrity and dynamic properties of the microtubule cytoskeleton are indispensable for the development of the mammalian brain. Consequently, mutations in the genes that encode the structural component (the α/β-tubulin heterodimer) can give rise to severe, sporadic neurodevelopmental disorders. These are commonly referred to as the tubulinopathies. Here we report the addition of recessive quadrupedalism, also known as Uner Tan syndrome (UTS), to the growing list of diseases caused by tubulin variants. Analysis of a consanguineous UTS family identified a biallelic *TUBB2B* mutation, resulting in a p.R390Q amino acid substitution. In addition to the identifying quadrupedal locomotion, all three patients showed severe cerebellar hypoplasia. None, however, displayed the basal ganglia malformations typically associated with *TUBB2B* mutations. Functional analysis of the R390Q substitution revealed that it did not affect the ability of β-tubulin to fold or become assembled into the α/β-heterodimer, nor did it influence the incorporation of mutant-containing heterodimers into microtubule polymers. The 390Q mutation in *S. cerevisiae TUB2* did not affect growth under basal conditions, but did result in increased sensitivity to microtubule-depolymerizing drugs, indicative of a mild impact of this mutation on microtubule function. The *TUBB2B* mutation described here represents an unusual recessive mode of inheritance for missense-mediated tubulinopathies and reinforces the sensitivity of the developing cerebellum to microtubule defects.

[†]Current Address: Institute of Science and Technology Austria, Am Campus 1, 3400 Klosterneuburg, Austria.
Received: September 12, 2016. **Revised:** October 17, 2016. **Accepted:** November 3, 2016

Introduction

Microtubules fulfil a wide variety of critical functions throughout the development of the mammalian brain (1,2): they form the mitotic spindle, provide a framework during cellular migration and process extension and provide a stable platform for intracellular transport. Defects in these processes can result in various neurological disorders, including primary microcephaly (*e.g. ASPM*) and lissencephaly (*e.g. PAFAH1B1*) (1–6).

Over the past decade, a plethora of mutations in genes encoding the building blocks of microtubules themselves, the tubulins, have been associated with neurodevelopmental diseases that are now referred to as the tubulinopathies (2,7,8). Out of the 19 human genes encoding the α-, β- and γ-tubulin isoforms, variants in 11 (*TUBA1A*, *TUBA4A*, *TUBA8*, *TUBB1*, *TUBB2A*, *TUBB2B*, *TUBB3*, *TUBB5*, *TUBB4A*, *TUBB8* and *TUBG1*) have been implicated in human disorders, the majority affecting the central nervous system (8–22). To date, more than 100 distinct mutations have been reported in the various tubulin genes, covering a wide spectrum of human conditions from lissencephaly to ALS and female sterility (7,9,12,14). This diversity can also be seen on the single gene level. For instance, distinct mutations in *TUBB3* can cause either polymicrogyria (*e.g.* E205K) or axon guidance disorders (*e.g.* R262C), depending on the variant's impact on microtubule function (18,17).

Despite this variability, the neurodevelopmental tubulinopathies often share certain characteristics. Phenotypically, patients with mutations in these tubulin genes frequently show supratentorial defects such as neuronal migration disorders of the cerebral cortex, agenesis of the corpus callosum and perturbation of the basal ganglia, as well as hypoplasia and malformations of the hindbrain (2,7). Although specific phenotypes may be more frequently associated with one isoform (*e.g. TUBA1A* to lissencephaly or *TUBB2B* to polymicrogyria), overall, many of the isoforms (*TUBA1A*, *TUBB2A*, *TUBB2B*, *TUBB3* and *TUBB5*) converge on a spectrum of related disorders (7,20,23).

Genetically, almost all of the disease-causing tubulin mutations described are sporadic and autosomal dominant, the exceptions being a homozygous splice-mutation in *TUBA8* of unclear relevance and recently reported homozygous *TUBB8* variants that cause female sterility (2,7,20,24,25).

Uner Tan syndrome (also known as Cerebellar Ataxia, Mental Retardation, And Dysequilibrium Syndrome, CAMRQ) is a collection of recessive single gene disorders, in which affected individuals show quadrupedalism, mental retardation and cerebellar developmental defects (26–29). To date, mutations in *VLDLR*, *WDR81*, *CA8* and *ATP8A2* have been described as causative in this disease (26–29).

Here we report the discovery of a homozygous *TUBB2B* variant that segregates with a familial case of Uner Tan syndrome (UTS) with cerebellar hypoplasia. Heterozygous mutations in this gene were originally described in cases of asymmetric polymicrogyria in association with basal ganglia defects and various degrees of microcephaly, corpus callosum abnormalities and hindbrain defects (19). With the present study, we expand the list of diseases caused by tubulin mutations and also demonstrate the possibility of recessive inheritance of pathogenic tubulin mutations in neurodevelopmental disease.

Results

Description and genetic analysis of an extended Uner Tan syndrome family

We previously described three living, affected individuals of an extended Turkish family with UTS (Table 1 and Fig. 1A–E) (30). All three presented with identical quadrupedal locomotion in combination with mild to severe ataxia and intellectual disability. Patients were from both branches of a two-branch consanguineous pedigree, suggesting a recessive cause. At last examination as adults, the head circumference was reduced (-3.32 SD to -5.78 SD), gross and fine motor development were delayed in all afflicted individuals, and language and social development were either absent (III-7 and III-8) or delayed (III-4) (31). There were no reports of seizures. All three individuals showed extensive cerebellar hypoplasia; two also showed simplified cortical gyration (Fig. 1B). With the exception of the corpus callosum in III-4, other brain regions were structurally intact.

As mutations in *VLDLR*, a previously reported cause of UTS, were absent, whole exome sequencing was performed for all three affected individuals (26,30). Analysis of the sequencing data employing our standard prioritization pipeline resulted in the identification of only one shared candidate mutation, located in the tubulin isoform *TUBB2B* (32). This variant, a c.1169G > A (RefSeq: NM_178012.4) conversion, resulting in a p.390R > Q substitution, segregated with the recessive phenotype in the three affected individuals, the mothers of both branches (II-2 and II-4) and non-UTS siblings (III-3, III-6, III-9, III-12 and III-13) (Fig. 1A and F and Supplementary Material, Fig. S1); it was also located in a block of homozygosity shared by all three UTS patients as analysed by HomozygosityMapper (Supplementary Material, Fig. S2) (33,34).

This variant was not present in the GME Variome or the ExAC database and was annotated as disease-causing by internal tools and the program MutationTaster (32,35,36). The affected arginine at position 390 is located in the C-terminal domain of TUBB2B and is highly conserved in vertebrate and invertebrate homologs (Fig. 1F and G). The sole β-tubulin found in *S. cerevisiae*, Tub2p, does not contain an encoded arginine at this position, but has a similar positively charged lysine residue at this position.

Location and impact of the R390Q variant on folding and integration

Because of the intriguing recessive mode of inheritance for this tubulin mutation, we sought to gain insight into the resulting pathogenic mechanisms via structural modelling. This analysis revealed that R390 resides on the surface of the protein and is part of the longitudinal inter-dimer interface (Fig. 2) (37). Together with R391 and K392, it forms a three-pronged basic structure that binds to the adjacent α-tubulin within the protofilament. This interface is also important for the interaction with maytansine and related drugs that impair the linear assembly of heterodimers, suggesting that alterations of the β-tubulin surface at this position might interfere with the dynamic properties of microtubules (38).

The *de novo* generation of tubulin heterodimers is dependent on the concerted action of multiple chaperones, including five that are exclusive for this pathway (39). To investigate the

Table 1. Clinical details

	III-4	III-7	III-8
Mutation	p.Arg390Gln	p.Arg390Gln	p.Arg390Gln
Gender	male	male	female
Country of origin	Turkey	Turkey	Turkey
Psychomoter Development			
Gross motor (normal/delayed/absent)	delayed	delayed	delayed
Fine motor (normal/delayed/absent)	delayed	delayed	delayed
Language (normal/delayed/absent)	delayed	absent	absent
Social (normal/delayed/absent)	delayed	absent	absent
Neurological Examination			
Age at last examination	28	25	20
HC at last examination cm (SD)	52 cm (-3.80 SD)	49 cm (-5.78 SD)	52 cm (-3.32 SD)
Hypotonia	infantile	infantile	infantile
Hyperreflexia	lower extremities	lower extremities	lower extremities
Truncal ataxia	+ (mild)	+ (severe)	+ (severe)
Gait ataxia	+ (mild)	+ (severe)	+ (severe)
Intention tremor	+ (mild)	–	–
Dysarthria	+	nonverbal	nonverbal
Dysmetria	+ (mild)	+	+
Dysdiadochokinesis	+ (mild)	+	+
Intellectual disability	+ (moderate)	+ (severe)	+ (severe)
Quadrupedal locomotion	+	+	+
Seizures			
Seizures	–	–	–
Ophthalmologic findings			
Strabismus	–	–	–
Cataracts (postnatal)	–	–	–
Gaze-evoked nystagmus	horizontal	–	vertical
Musculoskeletal findings			
Wide and short nape of neck	–	–	–
Flexion of skull towards the spine	–	–	–
Thoracic kyphosis	–	–	–
Thoracic scoliosis	–	–	–
Pes planus	+	+	–
MRI findings			
Generalized cerebral atrophy	–	–	–
Pachygyria	–	–	–
Polymicrogyria (perisylvian/multifocal/generalized)	–	–	–
Cortical gyral simplification	+	+	–
Cerebellar hypoplasia/atrophy	+	+	+
Aplasia/dysplasia/hypoplasia of the inferior cerebellar vermis	+	+	+
Hypoplasia of the brainstem	–	–	–
Hypoplasia/atrophy of the corpus callosum	+	–	–
Atrophy of the dentate nucleus	–	–	–
Basal ganglia abnormalities	–	–	–

potential impact of the R390Q variant, we employed radioactive labelling of wild-type and mutant protein in coupled transcription/translation reactions and analysed the kinetics of target protein/chaperone complex formation. These experiments revealed no differences in either polypeptide translational efficiency, the kinetics of folding or the end-point yield of newly assembled heterodimers (Fig. 3A and B).

Because the R390 residue is part of an important binding interface with α-tubulin contained in an adjacent heterodimer, we reasoned that the mutation might affect incorporation into the microtubule lattice. To assess this *in vivo*, FLAG-tagged wild-type and mutant Tubb2b were expressed in HEK293T cells and stained with antibodies to detect α-tubulin and the overexpressed constructs (Fig. 3C–H). Wild-type and mutant proteins showed indistinguishable co-localisation with the endogenous microtubule cytoskeleton, suggesting no difference in the ability of the mutant to polymerize into microtubules. These data were confirmed in parallel experiments using COS-7 cells (Supplementary Material, Fig. S3).

Introduction of the 390Q mutation impacts microtubule stability in yeast

While the R390Q mutation did not affect folding and integration, these two assays could not address its potential effect on microtubule stability. We decided to interrogate this possibility using the budding yeast *S. cerevisiae*. Its sole β-tubulin Tub2p and human TUBB2B share 74% amino acid sequence identity and show 84% similarity when charge-maintaining

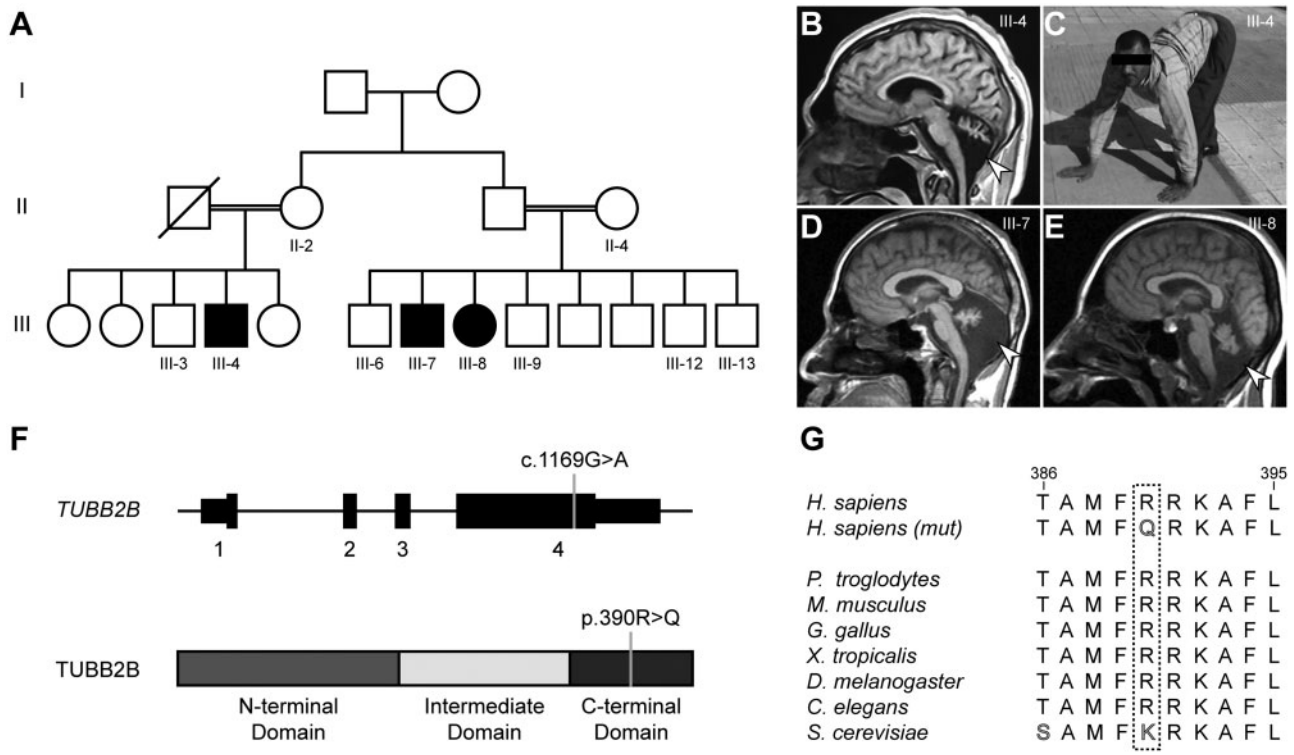

Figure 1. An extended Uner Tan syndrome family harbours a recessive mutation in *TUBB2B*. (**A**) Family tree with two branches of the previously reported family (30). Double lines: reported consanguinity. Filled symbols: affected individuals. Family tree was simplified relative to the previously published version and omits unaffected and affected deceased children from generation III. (**B**) Sagittal MRI image of patient III-4. (**C**) Image of patient III-4 using all four limbs for locomotion, the diagnostic hallmark of Uner Tan Syndrome. (**D,E**) Sagittal MRI images of patients III-7 and III-8, respectively. Arrowheads in B, D and E indicate severe cerebellar hypoplasia for all patients. Images similar to B–E have been published previously (30). (**F**) Upper model depicts the *TUBB2B* coding sequence spanning four exons and the 5' and 3' UTRs. Grey line indicates the position of the c.1169G > A mutation (RefSeq: NM_178012.4). Lower model depicts the TUBB2B protein sequence with the three tubulin domains (N-terminal, intermediate and C-terminal). Grey line indicates the position of the resulting p.390R > Q amino acid substitution (RefSeq: NP_821080.1). (**G**) Residue p.R390 is conserved in homologs of all vertebrates, *D. melanogaster* and *C. elegans*. The budding yeast homolog Tub2p shows conservation of the positive charge by an encoded lysine residue in place of arginine.

substitutions are considered as conserved (40). Due to the relatively simple introduction of transgenic variants, *S. cerevisiae* is a convenient and established model for testing the impact of β-tubulin mutations on microtubule stability (9,18,41).

As the R390Q mutation is recessive, we decided to use standard gene replacement methods to introduce the homologous variant, K390Q, into the haploid yeast strain BY4741 (42,43). Control *TUB2.URA3* and mutant *tub2-K390Q.URA3* strains were recovered at similar frequencies, indicating that the *tub2-K390Q* mutation was not lethal and neither strain showed any growth defects on YPD plates (Fig. 4A). However, the two strains exhibited differences when exposed to the microtubule destabilizing drugs nocodazole or benomyl (Fig. 4B–D). Previous work has shown that disease-causing mutations in tubulin often result in higher sensitivity to these drugs (9,18). Whereas the wild-type *TUB2.URA* strain behaved identically to the parental strain when challenged with these two compounds, the mutant *tub2-K390Q.URA* strain showed reduced growth in a spot assay (Fig. 4B–D). We conclude that while the glutamine at position 390 did not affect the generation of the tubulin heterodimer or its ability to polymerize into microtubules, it impaired microtubule stability *in vivo*.

Expression of *Tubb2b* in the developing embryonic cerebellum

Because of the pronounced cerebellar phenotype observed in the affected individuals, we investigated the expression of the mouse homolog Tubb2b in this brain region during embryonic development. We previously generated and characterized a BAC-transgenic mouse line that expresses GFP under the control of the endogenous *Tubb2b* locus (44). This strategy was necessary due to a lack of validated antibodies that are specific for Tubb2b. Our previous analysis focused on the postnatal developing cerebellum, where we could detect widespread GFP signal in progenitors and post-mitotic neurons (44). Here, we extended this approach to the embryonic stages, as the extensive cerebellar hypoplasia observed in UTS patients as well as hindbrain malformations in other tubulinopathy patients may be a result of defects during early development.

Tubb2b was widely expressed throughout the nervous system and can also be seen at high levels in the developing cerebellar anlage at embryonic day 16.5 (Fig. 5A–C). The GFP signal was weaker in the external granular zone (EGZ) compared with the Purkinje cell cluster area (PCC), although still clearly above background fluorescence in controls (Fig. 5D–F). This was

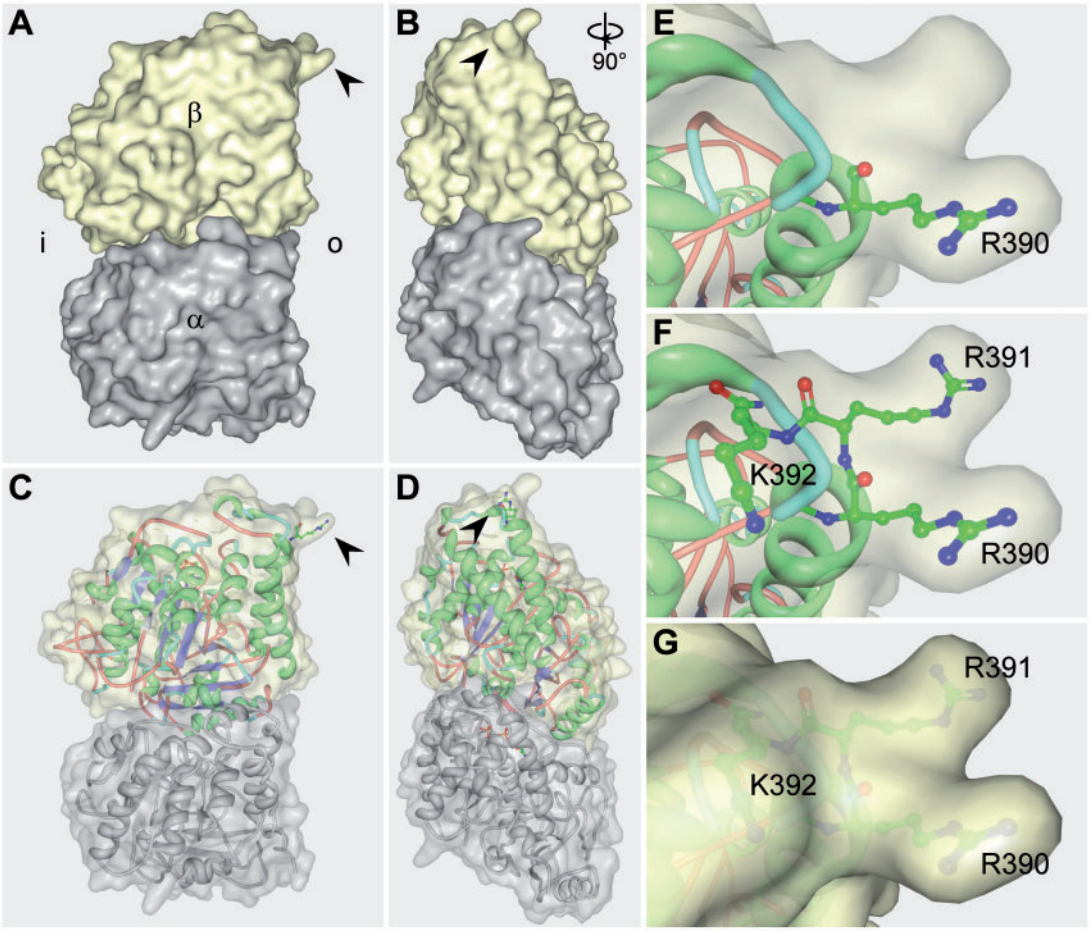

Figure 2. Location of the R390 residue within the tubulin heterodimer. (**A–G**) Depiction of the 2D electron crystallography of the tubulin heterodimer using a previously published data set (RCSB PDB: 1JFF) (37). (A–D) Overview of the tubulin heterodimer in lateral (A and C) and frontal views (B and D), relative to their position in an assembled microtubule. Shown are a surface model (A,B) and a mixed surface and ribbon model (C,D). Arrowheads indicate the location of the R390 residue. α: α-tubulin; β: β-tubulin; i: heterodimer surface facing the inside (lumen) of the microtubule; o: heterodimer surface facing outwards in a microtubule. (E–G) Magnified view of the R390 residue (E) and the adjacent positively charged R391 and K392 residues (F,G). These three positively charged amino acids form a binding pocket that interacts with the α-tubulin of the longitudinally adjacent tubulin-heterodimer.

consistent with our previous observation that *Tubb2b* is expressed at lower levels in proliferating cells (44). More detailed analysis revealed that *Tubb2b* was present in Pax6-positive progenitors in the EGZ and developing excitatory neurons in the PCC (99.24% ± 0.13%; $n = 3$ animals, 652 cells), pH3-positive mitotic cells (98.98% ± 1.01%; $n = 3$ animals, 99 cells), NeuN-positive post-mitotic neurons (98.88% ± 1.12%; $n = 3$ animals, 530 cells), Calbindin-positive Purkinje cells (99.32% ± 0.67%; $n = 3$ animals, 286 cells) and Sox2-positive progenitors in the ventricular zone and Bergmann glial cells in the PCC (99.76% ± 0.24%; $n = 3$ animals, 415 cells) (Fig. 5G–Z). Taken together, these data demonstrate that *Tubb2b* is abundantly expressed throughout the development of the cerebellum, and, just as in cortical development, can be found in all known cell types found in the cerebellar anlage at this embryonic time point.

Discussion

In this study, we describe the identification of a recessive *TUBB2B* mutation that segregated within a family diagnosed with Uner Tan syndrome. This variant was the only identified candidate locus that passed our filters and was shared between the three patients, all of whom exhibited the stereotypic quadrupedal locomotion and severe cerebellar hypoplasia. The resulting p.R390Q amino acid substitution did not affect the ability to fold and integrate into the microtubule lattice; however, its homologous variant in yeast sensitized cells to microtubule-destabilizing drugs.

TUBB2B is the fifth gene that has been implicated in UTS. Similar to the others, *VLDLR*, *ATP8A2*, *WDR81* and *CA8*, the causative mutation is familial and recessive (26–29). Phenotypically, *TUBB2B* patients resemble those with mutations in the former three, as these cases present with cerebellar hypoplasia and impact the size, structure or both of the cerebral cortex (26–28). This is reflected in mouse models for loss of *Vldlr* and *Atp8a2*, even though the latter showed progressive ataxia in the wabbler-lethal animals (45,46). No imaging has been provided for the *CA8* patients (29); however, a mouse model for this gene has shown no alteration in cerebellar and cerebral structure or size (47).

The phenotypic convergence of all genes on quadrupedal locomotion and mental impairment could suggest that they are involved in a common mechanism or pathway. However, this

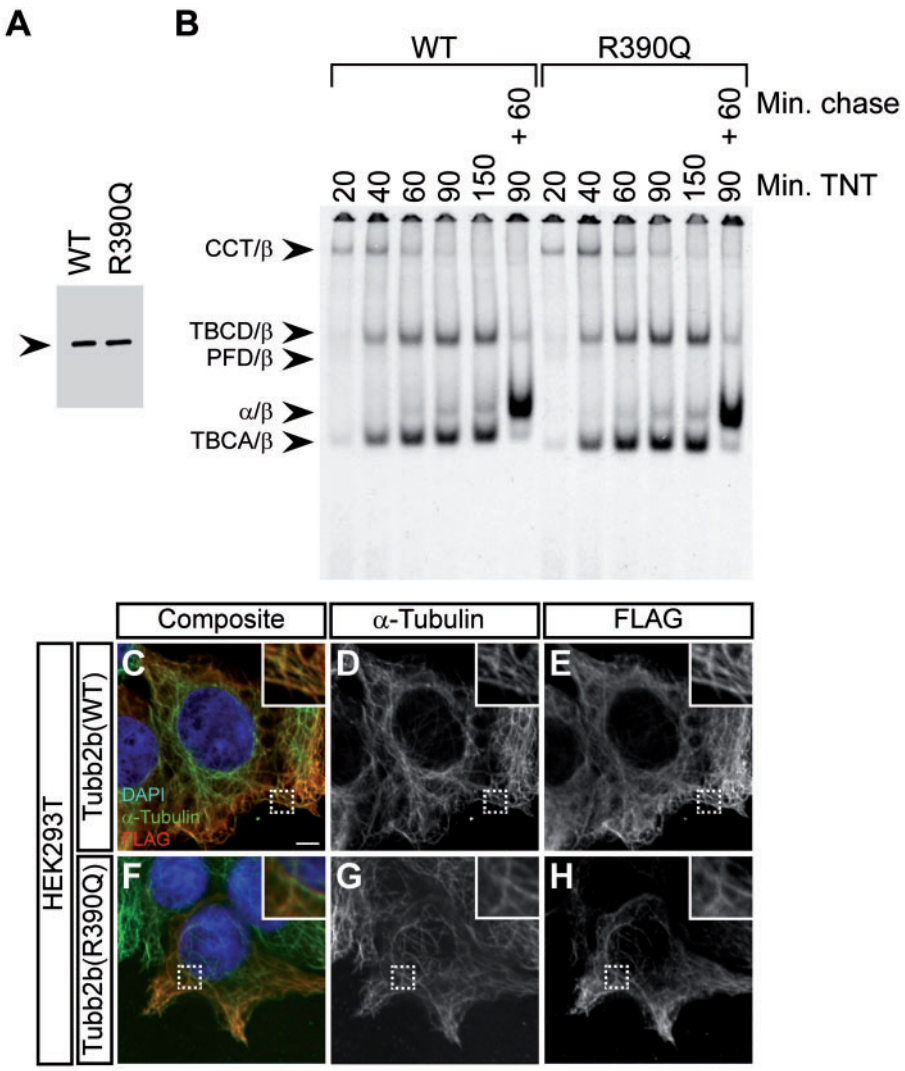

Figure 3. The R390Q mutation does not affect tubulin folding or heterodimer integration into the microtubule lattice (**A**) Denaturing gel of *in vitro* transcribed and translated reaction products for wild-type (WT) and the TUBB2B R390Q mutant, in which the ^{35}S-methinonine labelled proteins were detected by autoradiography. Note that the translational efficiency is not affected by the mutation. Arrowhead indicates the β-tubulin band. (**B**) Kinetic analysis of tubulin folding on non-denaturing gels of wild-type and R390Q translation products. Arrowheads (from top to bottom) denote the following complexes: chaperonin (CCT)/β-tubulin binary complex, the TBCD/β-tubulin co-complex, the prefoldin (PFD)/β-tubulin complex, the native tubulin heterodimer and the TBCA/β-tubulin co-complex. The molecular identities are assigned on the basis of their characteristic electrophoretic mobility. Shown are lanes for different reaction times (20, 40, 60, 90 and 150 minutes) in the rabbit reticulocyte lysate (TNT) and a combination of 90 minutes TNT and 60 minutes of chase with unlabelled wild-type tubulin. The R390Q mutation does not affect the kinetics of tubulin heterodimer formation or endpoint yields. (**C–H**) Immunofluorescence images of HEK293T cells transfected with FLAG-tagged wild-type Tubb2b (C–E) or mutant R390Q (F–H) and stained with antibodies against α-tubulin and the FLAG-tag. Shown are composite images (C and F) and grey-scale images of the individual channels (D, E, G and H). Wild-type and mutant tubulin heterodimers are both capable of integration into the microtubule lattice. Scale bar in (C) shows 5 μm. Magnifications of the dashed rectangles are shown in the upper right corner of each image.

does not seem to be the case. Whereas *TUBB2B* encodes a structural component of the cytoskeleton, none of the other genes are related to either this function or to each other. VLDLR is a reelin receptor and its knockout in mouse impairs downstream signalling through Dab1 (46); ATP8A2 is an aminophospholipid transporter and its depletion in mouse causes axonopathy (46,48). The function of the transmembrane protein WDR81 is poorly understood, but a recent mouse study has suggested a role in Purkinje cell survival, its localization to mitochondria and its importance in their integrity (49). Finally, CA8 is important for the modulation of Ca^{2+} signalling in Purkinje cells and its perturbation in mouse results in defective GABAergic signalling (50). Based on the human and functional data, we propose a tentative distinction between three types of UTS based on their clinical presentation rather than their disease mechanism: 1) developmental UTS (*TUBB2B*, *VLDLR*); 2) degenerative UTS (ATP8A2, WDR81); and 3) UTS without cerebellar malformations (*CA8*). However, the latter still has to be confirmed by future imaging of human patients and is currently based solely on mouse data.

Previously reported amino acid substitutions in tubulin encoding genes that caused neurological disease were exclusively heterozygous and, with the exception of mosaic parents, occurred in sporadic cases (2,7,51). This is the first case of a recessively inherited mutation in this gene family, with the exception of a splice site alteration in *TUBA8*, the relevance of which is still unclear, and homozygous mutations in *TUBB8* that cause female sterility (20,25,52).

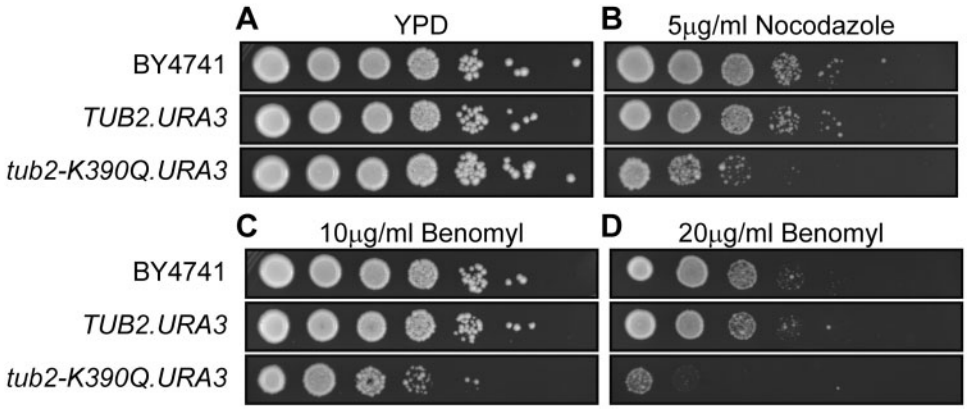

Figure 4. Introduction of the K390Q mutation into the single budding yeast β-tubulin gene results in increased sensitivity to microtubule destabilizing drugs. (**A–D**) Spot assays showing a logarithmic dilution series for the original wild-type strain (BY4741) and derivatives in which the normal *TUB2* locus was replaced by either *TUB2.URA3* or *tub2-K390Q.URA3*. Cells grow normally on YPD (A), but show increased sensitivity to nocodazole (B) and benomyl (C,D), suggesting decreased microtubule stability in the presence of tubulin-heterodimers with the K390Q amino acid substitution.

We and others originally proposed that tubulinopathies can be caused by haploinsufficiency, as the impaired folding of many variants suggested reduced heterodimer abundance (8,53,54). However, the identification of *TUBB3* mutations that can cause different disease phenotypes and the lack of true haploid loss-of-function mutations has cast doubt on this hypothesis (17,18,55). This led Kumar and colleagues to propose a model in which all tubulin mutations would act by a gain-of-function, rather than a (partial) loss-of-function (55). It is apparent, however, that the situation is more complex.

Our previous work on the β-tubulin isoform *TUBB5* showed that heterozygous missense mutations in this gene – which is expressed at high levels throughout brain development – cause microcephaly with structural brain abnormalities (14,56,57). While overexpression of disease-causing TUBB5 mutants resulted in migration and progenitor defects *in utero*, so did Tubb5 depletion (14,56). Moreover, heterozygous loss in a conditional knockout resulted in severe microcephaly, one of the main patient phenotypes (57). We note, however, that analysis of a disease-causing knockin showed some additional, milder phenotypes that were absent in the knockout and that may contribute to the disease presentation. This suggests that tubulinopathies do not all act by a simple loss or gain of function, but can result from a combination of the two. The existence of a recessive variant alongside the heterozygous mutations further supports this notion.

The cases we describe here also exhibit a unique presentation within the tubulinopathies. Although gyral simplification and cerebellar hypoplasia are well within the described spectrum, the combination of severe cerebellar hypoplasia together with a relatively mild cortical phenotype are quite rare, and have only recently been described (7,51). More striking is the absence of basal ganglia defects in all three patients, normally considered a hallmark of the neurological tubulinopathies (2). Oegema and colleagues described heterozygous mutations in *TUBB2B* in cases of cerebellar hypoplasia in the presence of mild cortical malformations (51). Although these individuals overlap phenotypically with the UTS patients described here, they also exhibit malformations of the basal ganglia, distinguishing these two cohorts.

This distinction coincides with a different inheritance pattern, suggesting that the cerebellum is exquisitely sensitive to a specific change in microtubule function. A similar dichotomy arises with respect to *TUBB3* mutations: one class causes increased stabilization and polymerization of microtubules and results in congenital fibrosis of the extraocular muscles (CFEOM3) and basal ganglia defects in the absence of cortical and cerebellar malformations; the other class negatively impacts stability and is strongly associated with cerebral and cerebellar malformations (18,17). It is unclear which developmental mechanism or cell type in the cerebellum might render its formation more sensitive to tubulin destabilization compared with other brain regions.

How does the R390Q variant differ from previously reported amino acid substitutions in *TUBB2B*? Its recessive inheritance, the unusual combination of presence and absence of brain malformations and quadrupedal locomotion sets it apart from other human mutations in this gene. It also contrasts with a previously reported recessive mouse model harbouring an ENU-induced *Tubb2b* mutation that results in an N247S amino acid substitution (58): homozygous mice did not survive past birth, and heterozygous mice showed mild cortical phenotypes with behavioural abnormalities.

Whereas cerebellar malformations have been previously described for patients with *TUBB2B* variants, these did not present with quadrupedal locomotion (7,51). This phenotypic difference may arise from qualitative or quantitative differences in cerebellar malformations. Alternatively, differences in the connectivity between or lesions within cortical motor control centres that are undetectable by MRI may underlie this phenomenon. These questions could be addressed by histopathological examinations, alternative imaging methods that allow analysis of activity and brain wiring or the use of mouse models introducing the different human mutations.

However, this would not address the molecular and cellular pathologies that might be unique to the R390Q variant. This residue is not altered in any other reported tubulinopathy case involving β-tubulin; likewise, none of the other two basic amino acids that are directly adjacent to R390, R391 or K392, were implicated previously (2,7,9,25). Exchange of the first arginine with glutamine in this series most likely only reduces the affinity with the adjacent heterodimer, because this changes the charge but does not introduce a side chain that could sterically block the inter-dimer interaction (37). This notion is supported by the mutant's capability to integrate into the microtubule lattice in our functional assay. Because introduction of a homologous

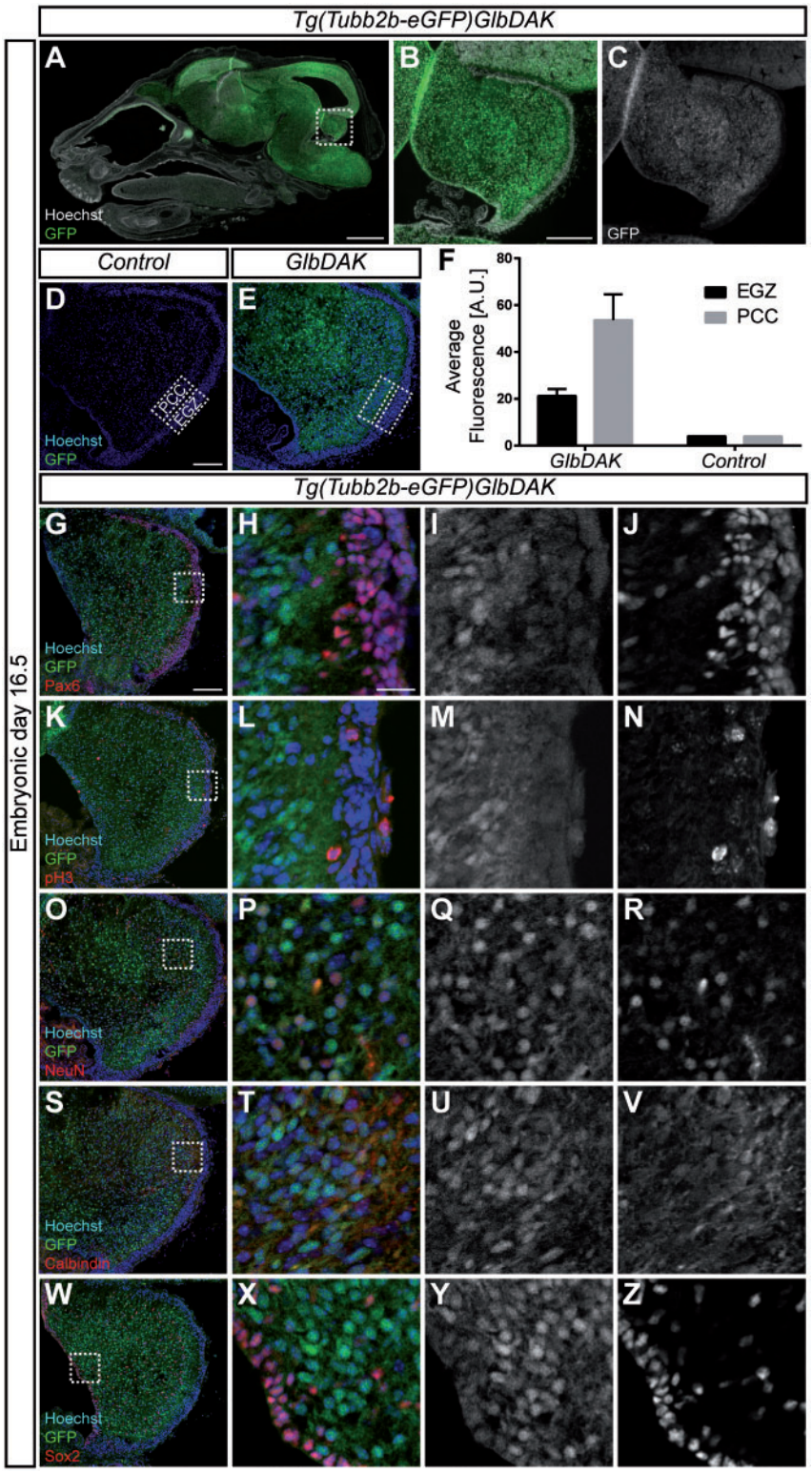

Figure 5. Tubb2b is expressed at high levels in the embryonic cerebellum. (**A–C**) Overview scan of a sagittal section of an embryonic day (E) 16.5 head of the *Tg(Tubb2b-eGFP)GlbDAK* line. eGFP is expressed under the control of the endogenous *Tubb2b* locus on a bacterial artificial chromosome (BAC). (**B**) shows a magnification of the dashed rectangle encircling the cerebellar anlage in (A); in (C), the GFP channel is shown as a grey-scale image of (B). Hoechst staining for nuclear DNA is shown in white in A and B. (**D,E**) Confocal images of a control (D) and a transgenic animal (E). Hoechst staining for nuclear DNA is shown in blue in (D) and (E). PCC: Purkinje cell cluster area; EGZ: External Granular Zone. (**F**) Quantification of the average fluorescence intensity found in the EGZ and the PCC for control ($n = 1$) and transgenic mice ($n = 3$). For transgenic mice, mean ± SEM are shown. (**G–Z**) Fluorescent images of the developing cerebellum of the *Tg(Tubb2b-eGFP)GlbDAK* line at E16.5 stained for Pax6 (G–J), pH3 (K–N), NeuN (O–R), Calbindin (S–V) and Sox2 (W–Z). (H, L, P, T and X) show magnifications of the dashed rectangle in (G,K, O,S and W) respectively. (I, M, Q, U and Y), as well as (J, N, R, V and Z) show grey-scale images of the GFP and immunostaining channels, respectively. Scale bars show 1000 μm in A, 200 μm in B, 100 μm in (D) and (G) and 20 μm in (H).

mutation in yeast results in an increased sensitivity to microtubule depolymerizing drugs, we conclude that this variant causes decreased stability of the polymerized microtubule. Although such phenotypes have been described for other tubulin mutations, it is important to note that these assays have been performed in diploid, not haploid strains (9,18).

Our results therefore suggest that the R390Q mutation causes a mild destabilization of microtubules. Whereas its heterozygous occurrence does not visibly affect neurodevelopment, the homozygous presence of the mutation causes UTS. It is unclear whether this is a result of reaching a critical concentration of defective tubulin-heterodimers, or whether a specific lack of functional TUBB2B underlies this phenotype. This question has been an ongoing conundrum in the field of tubulin biology and is part of a larger controversy regarding the multi-tubulin hypothesis (2,59).

Our study demonstrates that recessive tubulin mutations can cause Uner Tan syndrome, extending both the spectrum of disease states and the mode of inheritance associated with the tubulinopathies.

Materials and Methods

Patient recruitment

The analysed family was enrolled using the locally approved protocols and was originally described elsewhere (30).

DNA extraction and whole exome sequencing

DNA was extracted on an Autopure LS instrument (Qiagen, Valencia, CA) with Autopure chemistry according to the manufacturer's instructions. Samples of the three affected individuals were subjected to Agilent Sure-Select Human All Exon v2.0 (44Mb baited target) library preparation and submitted for paired-end sequencing (2x76bp) on an Illumina HiSeq 2000. The accession number for these data is dbGAP: phs000288.v1.p1.

Computational analysis

Variant calling and filtering were performed according to our previously described whole exome sequencing pipeline (32). Variants were filtered if not present in all three affected, if the minor allele frequency (MAF) was >1:10,000, or if they yielded PolyPhen-2 prediction scores of <0.9 or GERP score <4.5. Cells were also checked with MutationTaster and homozygosity was confirmed using the tool HomozygosityMapper (33–35).

Sanger sequencing

Sanger sequencing of PCR products covering exon 4 of *TUBB2B* was performed using standard procedures (TUBB2B_PCR_F/R, TUBB2B_Seq_F/R; Supplementary Material, Table S1).

3D structural computation

The structure of the tubulin heterodimer was obtained from RCSB Protein Data Bank (http://www.rcsb.org/) and visualized using Protein Workshop (37,60).

In vitro tubulin folding assay

For *in vitro* transcription/translation reactions, plasmids engineered for the T7-driven expression of wild-type and R390Q TUBB2B were used to drive expression in rabbit reticulocyte lysate (TNT; Promega) containing ^{35}S-methionine as described (19,53). At the indicated intervals, aliquots were withdrawn and analysed on native polyacrylamide gels. For the final track shown on both gels, the reactions were supplemented (final concentration: 0.2 mg/ml) with native bovine brain tubulin after 90 minutes and the incubation continued for 60 minutes in order to drive the formation of native tubulin heterodimers.

Cell culture experiments and immunocytochemistry

HEK293T and COS-7 cells were maintained under standard sterile conditions in DMEM (Gibco, 11995-065), supplemented with 10% FBS (Gemini Bio-Products, 100-106) and 1% Pen Strep (Gibco, 15140-122). Prior and 4 hours after transfection, medium without the addition of Pen Strep was used. Cells were transfected with the Lipofectamine 2000 reagent according to the manufacturer's protocol (Thermo Scientific, 11668019). C-terminally FLAG-tagged cDNA encoding Tubb2b was cloned using the Keays lab internal mouse cDNA library (note that human TUBB2B and its murine homolog are 100% identical at the protein level). The R390Q mutation was introduced using the Q5 Site-Directed Mutagenesis Kit according to the manufacturer's instruction (NEB, E0554S; Tubb2b_Q5_F/R; Supplementary Material, Table S1). Constructs were transfected the day before methanol fixation and immunocytochemistry as described previously (8). The employed antibodies were: anti-DDDDK tag (Abcam, ab1162, 1:1000) and monoclonal anti-α-tubulin clone B-5 (Sigma-Aldrich, T6074-200UL, 1:1000). Cells were counterstained with DAPI (Thermo Fisher, D1306, 1:2000).

Generation of yeast strains and spot assays

Haploid BY4741 was the parental strain for generating the strains for studying the tub2-K390Q mutation. The pCS3 plasmid containing *TUB2* linked to a downstream *URA3* gene (*TUB2.URA3*) was a kind gift of the Gupta lab and was employed for the production of the wild-type *TUB2.URA* and mutant *tub2-K390Q.URA3* strains essentially as previously described (41,61). The K390Q mutation was introduced on the plasmid encoded *TUB2* gene by using a QuikChange Lightning Site-Directed Mutagenesis Kit according to the manufacturer's instructions (Agilent Technologies, 210518; TUB2_Quik_F/R; Supplementary Material, Table S1). The successful gene replacement was confirmed by PCR and Sanger sequencing (TUB2_PCR_F/R; Supplementary Material, Table S1) of genomic DNA (Gentra Puregene Yeast/Bact. Kit, Qiagen, 158567) according to standard methods. Tenfold dilutions of overnight cultures (30 °C) of the parental BY4741, wild-type *TUB2.URA3* and mutant *tub2-K390Q* strains were plated on YPD plates and YPD plates containing 5 μg/ml nocodazole (Sigma-Aldrich, M1404-2MG), 10 μg/ml benomyl (Sigma-Aldrich, 31586-5G) and 20 μg/ml benomyl. Spot assays were analysed following 48 hours of incubation at 30 °C.

Preparation and immunohistochemistry of mouse histological sections

Generation, breeding and histology of the *Tg(Tubb2b-eGFP)* mice were performed as described previously (44). Briefly, pregnant dams were sacrificed at embryonic day 16.5 and embryos were

dissected. Heads were drop-fixed in 4% PFA overnight, dehydrated in 30% sucrose, mounted in Neg-50 frozen section medium (Richard-Allan Scientific; 6502-APD) and sectioned (12 μm). Genotypes were confirmed by PCR and 3 positive, as well as one negative embryo, were used for the experiment. Overview images were acquired with a slide scanner (Zeiss), detailed scans of the cerebellum on a Zeiss LSM 700. Control sections were acquired at the same settings as *Tg(Tubb2b-eGFP)* tissue. The employed antibodies were: anti-Calbindin (Millipore, AB1778, 1:500), anti-NeuN (Millipore, MAB377, 1:400), anti-Pax6 (Covance, PRB-278P, 1:300), anti-pH3 (Millipore, MAB5654, 1:500) and anti-Sox2 (Santa Cruz Biotechnology, sc-17320). All experiments were done in 3 transgene positive animals. Sections were counterstained with DAPI (Thermo Fisher, D1306, 1:2000).

Quantification

For comparison of signal intensity between external granular zone and Purkinje cell cluster area in *Tg(Tubb2b-eGFP)* ($n = 3$) and control ($n = 1$) sections, the average intensity was measured in an area as indicated in the figure using ImageJ. The graph was generated using GraphPad Prism. For quantification of the proportion of GFP positive cells for each marker population, a 250x250 μm area was drawn and all cells within this area were assessed manually using ImageJ. The percentage of cells was determined for each animal and averaged. The presented data in the text are given as average ± SEM.

Supplementary Material

Supplementary Material is available at *HMG* online.

Acknowledgements

We are indebted to the patients and their family for their participation in this study. We want to thank M.L. Gupta and A. Luchniak for providing the pCS3 plasmid and Dr. Guoliang Chai for critical reading of the manuscript.

Conflict of Interest Statement. None Declared.

Funding

This work was supported by the US National Institutes of Health (grants P01HD070494, R01NS098004, and R01NS083823 for J.G.G; R01GM097376 for N.J.C.), the Simons Foundation for Autism Research (grant no. 275275; J.G.G.) and the Howard Hughes Medical Institute (J.G.G.). M.W.B. is supported by an EMBO Long-Term Fellowship (ALTF 174-2015), which is co-funded by the Marie Curie Actions of the European Commission (LTFCOFUND2013, GA-2013-609409). This work is partly supported by the Turkish Academy of Sciences, Ankara, Turkey.

References

1. Kuijpers, M. and Hoogenraad, C.C. (2011) Centrosomes, microtubules and neuronal development. *Mol. Cell. Neurosci.*, **48**, 349–358.
2. Breuss, M. and Keays, D.A. (2014) Nguyen, L. and Hippenmeyer, S. (eds.), In *Cellular and Molecular Control of Neuronal Migration*. Springer Netherlands, Dordrecht, in press., pp. 75–96.
3. Gleeson, J.G. and Walsh, C.A. (2000) Neuronal migration disorders: from genetic diseases to developmental mechanisms. *Trends Neurosci.*, **23**, 352–359.
4. Hu, W.F., Chahrour, M.H. and Walsh, C.A. (2014) The diverse genetic landscape of neurodevelopmental disorders. *Annu. Rev. Genomics Hum. Genet.*, **15**, 195–213.
5. Reiner, O. (2013) LIS1 and DCX: Implications for brain development and human disease in relation to microtubules. *Scientifica*, **2013**, 17.
6. Bond, J. and Woods, C.G. (2006) Cytoskeletal genes regulating brain size. *Curr. Opin. Cell Biol.*, **18**, 95–101.
7. Bahi-Buisson, N., Poirier, K., Fourniol, F., Saillour, Y., Valence, S., Lebrun, N., Hully, M., Bianco, C.F., Boddaert, N., Elie, C., *et al.* (2014) The wide spectrum of tubulinopathies: what are the key features for the diagnosis?. *Brain*, **137**, 1676–1700.
8. Keays, D.A., Tian, G., Poirier, K., Huang, G.J., Siebold, C., Cleak, J., Oliver, P.L., Fray, M., Harvey, R.J., Molnar, Z., *et al.* (2007) Mutations in alpha-tubulin cause abnormal neuronal migration in mice and lissencephaly in humans. *Cell*, **128**, 45–57.
9. Feng, R., Sang, Q., Kuang, Y., Sun, X., Yan, Z., Zhang, S., Shi, J., Tian, G., Luchniak, A., Fukuda, Y., *et al.* (2016) Mutations in TUBB8 and human oocyte meiotic arrest. *N. Engl. J. Med.*, **374**, 223–232.
10. Isrie, M., Breuss, M., Tian, G., Hansen, A.H., Cristofoli, F., Morandell, J., Kupchinsky, Z.A., Sifrim, A., Rodriguez-Rodriguez, C.M., Dapena, E.P., *et al.* (2015) Mutations in either TUBB or MAPRE2 cause circumferential skin creases Kunze type. *Am. J. Hum. Genet.*, **97**, 790–800.
11. Cushion, T.D., Paciorkowski, A.R., Pilz, D.T., Mullins, J.G., Seltzer, L.E., Marion, R.W., Tuttle, E., Ghoneim, D., Christian, S.L., Chung, S.K., *et al.* (2014) De novo mutations in the beta-tubulin gene TUBB2A cause simplified gyral patterning and infantile-onset epilepsy. *Am. J. Hum. Genet.*, **94**, 634–641.
12. Smith, B.N., Ticozzi, N., Fallini, C., Gkazi, A.S., Topp, S., Kenna, K.P., Scotter, E.L., Kost, J., Keagle, P., Miller, J.W., *et al.* (2014) Exome-wide rare variant analysis identifies TUBA4A mutations associated with familial ALS. *Neuron*, **84**, 324–331.
13. Simons, C., Wolf, N.I., McNeil, N., Caldovic, L., Devaney, J.M., Takanohashi, A., Crawford, J., Ru, K., Grimmond, S.M., Miller, D., *et al.* (2013) A de novo mutation in the beta-tubulin gene TUBB4A results in the leukoencephalopathy hypomyelination with atrophy of the basal ganglia and cerebellum. *Am. J. Hum. Genet.*, **92**, 767–773.
14. Breuss, M., Heng, J., Poirier, K., Tian, G., Jaglin, X., Qu, Z., Braun, A., Gstrein, T., Ngo, L., Haas, M., *et al.* (2012) Mutations in the β-tubulin gene TUBB5 cause microcephaly with structural brain abnormalities. *Cell Rep.*, **2**, 1554–1562.
15. Hersheson, J., Mencacci, N.E., Davis, M., MacDonald, N., Trabzuni, D., Ryten, M., Pittman, A., Paudel, R., Kara, E., Fawcett, K., *et al.* (2013) Mutations in the autoregulatory domain of beta-tubulin 4a cause hereditary dystonia. *Ann. Neurol.*, **73**, 546–553.
16. Lohmann, K., Wilcox, R.A., Winkler, S., Ramirez, A., Rakovic, A., Park, J.S., Arns, B., Lohnau, T., Groen, J., Kasten, M., *et al.* (2013) Whispering dysphonia (DYT4 dystonia) is caused by a mutation in the TUBB4 gene. *Ann. Neurol.*, **73**, 537–545.
17. Poirier, K., Saillour, Y., Bahi-Buisson, N., Jaglin, X.H., Fallet-Bianco, C., Nabbout, R., Castelnau-Ptakhine, L., Roubertie, A., Attie-Bitach, T., Desguerre, I., *et al.* (2010) Mutations in the neuronal ss-tubulin subunit TUBB3 result in malformation of cortical development and neuronal migration defects. *Hum. Mol. Genet.*, **19**, 4462–4473.

18. Tischfield, M.A., Baris, H.N., Wu, C., Rudolph, G., Van Maldergem, L., He, W., Chan, W.M., Andrews, C., Demer, J.L., Robertson, R.L., *et al.* (2010) Human TUBB3 mutations perturb microtubule dynamics, kinesin interactions, and axon guidance. *Cell*, **140**, 74–87.
19. Jaglin, X.H., Poirier, K., Saillour, Y., Buhler, E., Tian, G., Bahi-Buisson, N., Fallet-Bianco, C., Phan-Dinh-Tuy, F., Kong, X.P., Bomont, P., *et al.* (2009) Mutations in the beta-tubulin gene TUBB2B result in asymmetrical polymicrogyria. *Nat. Genet.*, **41**, 746–752.
20. Abdollahi, M.R., Morrison, E., Sirey, T., Molnar, Z., Hayward, B.E., Carr, I.M., Springell, K., Woods, C.G., Ahmed, M., Hattingh, L., *et al.* (2009) Mutation of the variant α-tubulin TUBA8 results in polymicrogyria with optic nerve hypoplasia. *Am. J. Hum. Genet.*, **85**, 737–744.
21. Poirier, K., Lebrun, N., Broix, L., Tian, G., Saillour, Y., Boscheron, C., Parrini, E., Valence, S., Pierre, B.S., Oger, M., *et al.* (2013) Mutations in TUBG1, DYNC1H1, KIF5C and KIF2A cause malformations of cortical development and microcephaly. *Nat. Genet*, **45,** 639–647.
22. Kunishima, S., Kobayashi, R., Itoh, T.J., Hamaguchi, M. and Saito, H. (2009) Mutation of the beta1-tubulin gene associated with congenital macrothrombocytopenia affecting microtubule assembly. *Blood*, **113**, 458–461.
23. Cushion, T.D., Dobyns, W.B., Mullins, J.G., Stoodley, N., Chung, S.K., Fry, A.E., Hehr, U., Gunny, R., Aylsworth, A.S., Prabhakar, P., *et al.* (2013) Overlapping cortical malformations and mutations in TUBB2B and TUBA1A. *Brain*, **136**, 536–548.
24. Braun, A., Breuss, M., Salzer, M.C., Flint, J., Cowan, N.J. and Keays, D.A. (2010) Tuba8 is expressed at low levels in the developing mouse and human brain. *Am. J. Hum. Genet.*, **86**, 819–822. author reply 822-813.
25. Feng, R., Yan, Z., Li, B., Yu, M., Sang, Q., Tian, G., Xu, Y., Chen, B., Qu, R., Sun, Z., *et al.* (2016) Mutations in TUBB8 cause a multiplicity of phenotypes in human oocytes and early embryos. *J. Med. Genet*, **53,** 662–671.
26. Ozcelik, T., Akarsu, N., Uz, E., Caglayan, S., Gulsuner, S., Onat, O.E., Tan, M. and Tan, U. (2008) Mutations in the very low-density lipoprotein receptor VLDLR cause cerebellar hypoplasia and quadrupedal locomotion in humans. *Proc. Natl. Acad. Sci.*, **105**, 4232–4236.
27. Onat, O.E., Gulsuner, S., Bilguvar, K., Nazli Basak, A., Topaloglu, H., Tan, M., Tan, U., Gunel, M. and Ozcelik, T. (2013) Missense mutation in the ATPase, aminophospholipid transporter protein ATP8A2 is associated with cerebellar atrophy and quadrupedal locomotion. *Eur. J. Hum. Genet.*, **21**, 281–285.
28. Gulsuner, S., Tekinay, A.B., Doerschner, K., Boyaci, H., Bilguvar, K., Unal, H., Ors, A., Onat, O.E., Atalar, E., Basak, A.N., *et al.* (2011) Homozygosity mapping and targeted genomic sequencing reveal the gene responsible for cerebellar hypoplasia and quadrupedal locomotion in a consanguineous kindred. *Genome Res.*, **21**, 1995–2003.
29. Turkmen, S., Guo, G., Garshasbi, M., Hoffmann, K., Alshalah, A.J., Mischung, C., Kuss, A., Humphrey, N., Mundlos, S. and Robinson, P.N. (2009) CA8 mutations cause a novel syndrome characterized by ataxia and mild mental retardation with predisposition to quadrupedal gait. *PLoS Genet.*, **5**, e1000487.
30. Tan, U. (2014) Two families with quadrupedalism, mental retardation, no speech, and infantile hypotonia (Uner Tan Syndrome Type-II); a novel theory for the evolutionary emergence of human bipedalism. *Front. Neurosci.*, **8**, 84.
31. Neyzi, O., Bundak, R., Gokcay, G., Gunoz, H., Furman, A., Darendeliler, F. and Bas, F. (2015) Reference Values for Weight, Height, Head Circumference, and Body Mass Index in Turkish Children. *J. Clin. Res. Pediatr. Endocrinol.*, **7**, 280–293.
32. Dixon-Salazar, T.J., Silhavy, J.L., Udpa, N., Schroth, J., Bielas, S., Schaffer, A.E., Olvera, J., Bafna, V., Zaki, M.S., Abdel-Salam, G.H., *et al.* (2012) Exome sequencing can improve diagnosis and alter patient management. *Sci. Transl. Med.*, **4**, 138ra178.
33. Seelow, D. and Schuelke, M. (2012) HomozygosityMapper2012–bridging the gap between homozygosity mapping and deep sequencing. *Nucleic Acids Res.*, **40**, W516–W520.
34. Seelow, D., Schuelke, M., Hildebrandt, F. and Nurnberg, P. (2009) HomozygosityMapper–an interactive approach to homozygosity mapping. *Nucleic Acids Res.*, **37**, W593–W599.
35. Schwarz, J.M., Rodelsperger, C., Schuelke, M. and Seelow, D. (2010) MutationTaster evaluates disease-causing potential of sequence alterations. *Nat. Methods*, **7**, 575–576.
36. Scott, E.M., Halees, A., Itan, Y., Spencer, E.G., He, Y., Azab, M.A., Gabriel, S.B., Belkadi, A., Boisson, B., Abel, L., *et al.* (2016) Characterization of Greater Middle Eastern genetic variation for enhanced disease gene discovery. *Nat. Genet.*, **48**, 1071–1076.
37. Lowe, J., Li, H., Downing, K.H. and Nogales, E. (2001) Refined structure of alpha beta-tubulin at 3.5 A resolution. *J. Mol. Biol.*, **313**, 1045–1057.
38. Prota, A.E., Bargsten, K., Diaz, J.F., Marsh, M., Cuevas, C., Liniger, M., Neuhaus, C., Andreu, J.M., Altmann, K.H. and Steinmetz, M.O. (2014) A new tubulin-binding site and pharmacophore for microtubule-destabilizing anticancer drugs. *Proc. Natl. Acad. Sci.*, **111**, 13817–13821.
39. Lewis, S.A., Tian, G. and Cowan, N.J. (1997) The alpha- and beta-tubulin folding pathways. *Trends Cell Biol.*, **7**, 479–484.
40. Altschul, S.F., Madden, T.L., Schaffer, A.A., Zhang, J., Zhang, Z., Miller, W. and Lipman, D.J. (1997) Gapped BLAST and PSI-BLAST: a new generation of protein database search programs. *Nucleic Acids Res.*, **25**, 3389–3402.
41. Gupta, M.L., Jr., Bode, C.J., Dougherty, C.A., Marquez, R.T. and Himes, R.H. (2001) Mutagenesis of beta-tubulin cysteine residues in Saccharomyces cerevisiae: mutation of cysteine 354 results in cold-stable microtubules. *Cell Moti.L Cytoskeleton*, **49**, 67–77.
42. Brachmann, C.B., Davies, A., Cost, G.J., Caputo, E., Li, J., Hieter, P. and Boeke, J.D. (1998) Designer deletion strains derived from Saccharomyces cerevisiae S288C: a useful set of strains and plasmids for PCR-mediated gene disruption and other applications. *Yeast*, **14**, 115–132.
43. Winston, F., Dollard, C. and Ricupero-Hovasse, S.L. (1995) Construction of a set of convenient Saccharomyces cerevisiae strains that are isogenic to S288C. *Yeast*, **11**, 53–55.
44. Breuss, M., Morandell, J., Nimpf, S., Gstrein, T., Lauwers, M., Hochstoeger, T., Braun, A., Chan, K., Sanchez Guajardo, E.R., Zhang, L., *et al.* (2015) The expression of Tubb2b undergoes a developmental transition in murine cortical neurons. *J. Comp. Neurol.*, **523**, 2161–2186.
45. Trommsdorff, M., Gotthardt, M., Hiesberger, T., Shelton, J., Stockinger, W., Nimpf, J., Hammer, R.E., Richardson, J.A. and Herz, J. (1999) Reeler/Disabled-like disruption of neuronal migration in knockout mice lacking the VLDL receptor and ApoE receptor 2. *Cell*, **97**, 689–701.
46. Zhu, X., Libby, R.T., de Vries, W.N., Smith, R.S., Wright, D.L., Bronson, R.T., Seburn, K.L. and John, S.W. (2012) Mutations in a P-type ATPase gene cause axonal degeneration. *PLoS Genet.*, **8**, e1002853.

47. Jiao, Y., Yan, J., Zhao, Y., Donahue, L.R., Beamer, W.G., Li, X., Roe, B.A., Ledoux, M.S. and Gu, W. (2005) Carbonic anhydrase-related protein VIII deficiency is associated with a distinctive lifelong gait disorder in waddles mice. *Genetics*, **171**, 1239–1246.
48. Coleman, J.A., Kwok, M.C. and Molday, R.S. (2009) Localization, purification, and functional reconstitution of the P4-ATPase Atp8a2, a phosphatidylserine flippase in photoreceptor disc membranes. *J. Biol. Chem.*, **284**, 32670–32679.
49. Traka, M., Millen, K.J., Collins, D., Elbaz, B., Kidd, G.J., Gomez, C.M. and Popko, B. (2013) WDR81 is necessary for purkinje and photoreceptor cell survival. *J. Neurosci.*, **33**, 6834–6844.
50. Lamont, M.G. and Weber, J.T. (2015) Mice deficient in carbonic anhydrase type 8 exhibit motor dysfunctions and abnormal calcium dynamics in the somatic region of cerebellar granule cells. *Behav. Brain. Res.*, **286**, 11–16.
51. Oegema, R., Cushion, T.D., Phelps, I.G., Chung, S.K., Dempsey, J.C., Collins, S., Mullins, J.G., Dudding, T., Gill, H., Green, A.J., *et al.* (2015) Recognizable cerebellar dysplasia associated with mutations in multiple tubulin genes. *Hum. Mol. Genet.*, **24**, 5313–5325.
52. Tischfield, M.A. and Engle, E.C. (2010) Distinct alpha- and beta-tubulin isotypes are required for the positioning, differentiation and survival of neurons: new support for the 'multi-tubulin' hypothesis. *Biosci. Rep.*, **30**, 319–330.
53. Tian, G., Jaglin, X.H., Keays, D.A., Francis, F., Chelly, J. and Cowan, N.J. (2010) Disease-associated mutations in TUBA1A result in a spectrum of defects in the tubulin folding and heterodimer assembly pathway. *Hum. Mol. Genet.*, **19**, 3599–3613.
54. Tian, G., Kong, X., Jaglin, X.H., Chelly, J., Keays, D. and Cowan, N.J. (2008) A pachygyria-causing alpha-tubulin mutation results in inefficient cycling with CCT and a deficient interaction with TBCB. *Mol. Biol. Cell*, **19**, 1152–1161.
55. Kumar, R.A., Pilz, D.T., Babatz, T.D., Cushion, T.D., Harvey, K., Topf, M., Yates, L., Robb, S., Uyanik, G., Mancini, G.M.S., *et al.* (2010) TUBA1A mutations cause wide spectrum lissencephaly (smooth brain) and suggest that multiple neuronal migration pathways converge on alpha tubulins. *Hum. Mol. Genet.*, **19**, 2817–2827.
56. Ngo, L., Haas, M., Qu, Z., Li, S.S., Zenker, J., Teng, K.S., Gunnersen, J.M., Breuss, M., Habgood, M., Keays, D.A., *et al.* (2014) TUBB5 and its disease-associated mutations influence the terminal differentiation and dendritic spine densities of cerebral cortical neurons. *Hum. Mol. Genet.*, **23**, 5147–5158.
57. Breuss, M., Fritz, T., Gstrein, T., Chan, K., Ushakova, L., Yu, N., Vonberg, F.W., Werner, B., Elling, U. and Keays, D.A. (2016) Mutations in the murine homologue of TUBB5 cause microcephaly by perturbing cell cycle progression and inducing p53-associated apoptosis. *Development*, **143**, 1126–1133.
58. Stottmann, R.W., Donlin, M., Hafner, A., Bernard, A., Sinclair, D.A. and Beier, D.R. (2013) A mutation in Tubb2b, a human polymicrogyria gene, leads to lethality and abnormal cortical development in the mouse. *Hum. Mol. Genet.*, **22**, 4053–4063.
59. Fulton, C. and Simpson, P.A. (1976) Goldman, R., Pollard, T. and Rosenbaum, J. (eds.), In *Cell Motility*. Cold Spring Harbor Publications, New York, in press., pp. 987–1005.
60. Moreland, J.L., Gramada, A., Buzko, O.V., Zhang, Q. and Bourne, P.E. (2005) The Molecular Biology Toolkit (MBT): a modular platform for developing molecular visualization applications. *BMC Bioinformatics*, **6**, 21.
61. Sage, C.R., Davis, A.S., Dougherty, C.A., Sullivan, K. and Farrell, K.W. (1995) beta-Tubulin mutation suppresses microtubule dynamics in vitro and slows mitosis in vivo. *Cell Moti.L Cytoskeleton*, **30**, 285–300.